The Synthesis of Thermochemically Stable Single Phase Lanthanum Titanium Aluminium Oxide

Peng Zhang, Kwang-leong Choy*

UCL Institute for Materials Discovery, University College London, Malet Place, London, WC1E 7JE, UK

* Corresponding author

E-mail address: k.choy@ucl.ac.uk.

Highlights

- Single phase $LaTi_2Al_9O_{19}$ (LTA) has been successfully synthesized by sol-gel method at relatively low temperature (1350^{o}C), something not previously investigated.
- The sol-gel synthesized LTA shows good thermochemical stability up to 1500^{o}C.
- Sol-gel synthesized LTA shows higher coefficients of thermal expansion than the solid state reaction synthesized LTA.
- LTA is a face centre monoclinic material which has a very complicated crystal structure formed by AlO_6 and TiO_6 octahedra, connected through AlO_4 tetrahedra and 12-fold-coordinated La^{3+} cations.

Abstract

Lanthanum titanium aluminium oxide ($LaTi_2Al_9O_{19}$, LTA) synthesized by solid state reaction has been proven to be a promising thermal barrier material. However, LTA synthesized via solid state reaction requires a high processing temperature of at least 1500^{o}C for 24h. In this paper, single phase LTA was synthesized by sol-gel at a lower temperature (1350^{o}C) and the process parameters, phase composition, and relative thermal properties were investigated. Two-step calcination was used to obtain fine LTA powders. According to X-ray diffraction, the best calcination temperature of sol-gel synthesized LTA is 1350^{o}C. XRD results also showed the thermochemical stability of sol-gel synthesized LTA, which does not react with Al_2O_3 up to 1500^{o}C, to be excellent. Compared to LTA synthesized by solid state reaction, sol-gel synthesized LTA has higher coefficients of thermal expansion (CTEs) which are circa 10.2×10^{-6} $^oC^{-1}$ at 950^{o}C, related to the size dependent characteristic of CTEs. Therefore, sol-gel synthesized LTA can be a promising candidate as a thermal barrier material on Ni-based superalloys.
Key words**:** Sol-gel process; Calcination; Thermal properties; Thermal expansion

1. Introduction

Thermal barrier coating systems, mainly consisting of thermal barrier coatings (TBCs), thermally grown oxides (TGO), bond coats, and metallic substrates, are

the main components of turbine blades and vanes. They can offer a 100 to 300^{o}C temperature gradient and promote the desired high operating temperatures (above 1100^{o}C) to significantly improve gas turbine engine efficiency [1]. However, the development of metallic bond coats has faced a bottleneck, particularly due to the cost, with the cooling systems also reaching their current technology limit. Therefore, the main focus in the development of aviation gas turbine systems is concentrated on the development of TBCs [1-4]. TBCs, as protective thermal insulation layers, are widely applied to protect gas turbine engine blades and vanes. The state-of-the-art industrial TBC material is 6-8 wt.% yttria stabilized zirconia (6-8YSZ), which can be used for over the long term at temperatures below 1200^{o}C. At higher temperatures, sintering behavior and phase transformation will reduce the strain tolerance in combination with the increase in Young's modulus and volume change during cooling, consequently reducing the thermal cycling lifetime of TBCs [5, 6]. Currently, there is a growing demand in increasing the operating temperature to increase the efficiency of gas turbine engines, hence alternative materials are required instead of YSZ. The selection of TBC materials should fulfil the following requirements: (1) high melting point, (2) low thermal conductivity, (3) no phase transformation up to operation temperature, (4) suitable CTEs matching the metallic components, (5) good thermochemical stability, (6) good sintering resistance, and (7) good corrosion and erosion resistance [7, 8]. Therefore, the development of new TBC materials has been confined to doped zirconia, pyrochlores, perovskites, and aluminates [7, 9].

Alternative refractory materials, such as $LaTi_2Al_9O_{19}$ (LTA), have received increasing attention and this material has been synthesized via solid state reaction. The complex crystal structure of LTA offers potentially low thermal

conductivity (circa. 2.3 W m^{-1} K^{-1} for LTA ceramic, 1400^{o}C). Studies of LTA prove that it has better thermochemical stability, phase stability, and sintering resistance, and lower thermal conductivity than YSZ, with comparable mechanical properties and CTEs as YSZ, except for low fracture toughness [9]. Not only can LTA be used as thermal barrier material, it can also be used as a luminescent material, such as the matrix of laser materials, due to the optical inertia of La^{3+} that does not have any electrons in the 4f shell. Nanoscience and nanotechnology offer the potential to improve the physical and mechanical properties of new and established engineering materials due to the extremely small grain size as compared to conventional materials on the micron level [10]. A significant number of studies report that nanostructured materials and coatings show an expected improvement in mechanical properties, as well as lower thermal conductivities and better sintering resistance [11-13]. Therefore, in current research, nanostructured single phase LTA was synthesized using the sol-gel method to allow control of the structure, stoichiometry and composition at a molecular level, with the relative crystal structure, thermochemical, and thermophysical properties all being investigated.

2. Experimental

LTA powders were prepared using the Pechini sol-gel method. $La(NO_3)_3 \cdot 6H_2O$ (≥99.9%, Sigma Aldrich), $Al(NO_3)_3 \cdot 9H_2O$ (≥99.9%, Sigma Aldrich), and Titanium Butoxide [$Ti(OC_4H_9)_4$, ≥99.9%, Sigma Aldrich] as original materials were dissolved in absolute ethanol by stoichiometric ratio and stirred until complete light yellow transparent sol was obtained. Then, citric acid as the complexing agent and polyethylene glycol (PEG200) as the surfactant were added into the sol and stirred for another 30 minutes. The reaction is simply described by Figure 1 and the following chemical reactions [14]:

$$La^{3+} + 2Ti^{4+} + 9Al^{3+} + 19O^{2-} \Rightarrow LaTi_2Al_9O_{19} \quad (1)$$

The sol was dried at 120°C to form xerogel, calcined at the target temperature for 2h and ball milled for 24h to get fine white LTA powders. The as-prepared powders were pressed to corresponding bulk materials under 400MPa of the pressure, followed by calcination at 1300°C for 2h to densify the bulks.

The phases were characterized by X-ray diffractometer (XRD, SIEMENS Kristalloflex 810 diffractometer) with Cu-Kα radiation at a scan rate of 1.2°/min from 20° to 80°. The crystallite size was obtained by the refined X-ray diffractograms by using the Rietveld method. The morphology of powders was characterized by Scanning Electron Microscope (SEM, XL-30 FEG, Philips) and Transmission Electron Microscope (TEM, JEOL 2000FX). The CTEs were measured using a high-temperature dilatometer (TA Q400, TA Instrument) from ambient temperature to 950°C at a heating rate of 5°C/min. The LTA powders were mixed with Al_2O_3 with the volume ratio of 1:1 and pressed under the 400MPa of pressure, before being calcined at 1500°C to investigate the thermochemical stability.

3. Results and Discussion

3.1. The analysis of TGA-DSC curves of LTA xerogel

The calcination process of sol-gel produced LTA is determined by the DSC-TGA curves shown in Figure 2. According to the TGA curve in Figure 2, the weight loss of LTA xerogel begins at around 125°C, showing a huge decrease until 621°C and only a slight weight loss when above 621°C. The huge weight loss starting at 125°C can be attributed to the loss of water, the decomposition of organics, and the decomposition of nitrate ion, whilst the slight weight loss above 621°C may be due to the effect of purged gas and the crystallization of LTA, which also indicates that the decomposition of organics has been

completed at 621°C. The DSC curve shows a small and broad endothermic peak at 125°C, corresponding to the loss of water, with another endothermic peak around 276°C that corresponding to the decomposition of organics where a huge weight loss is shown in the TGA curve, mainly caused by the vigorous evolution of CO_2 of citric acid decomposed to aconitic acid ($C_6H_4O_6$) and itaconic acid ($C_5H_4O_4$) according to the following equation [15-17]:

$$citric\ acid \xrightarrow{175^oC} aconitic\ acid\ (C_6H_4O_6) + H_2O_{(g)} \quad (2)$$

$$aconitic\ acid \xrightarrow{heat} itaconic\ acid\ (C_5H_4O_4) + CO_{2(g)} \quad (3)$$

$$itaconic\ acid \xrightarrow{heat} itaconic\ anhydride\ (C_5H_4O_3) + H_2O \quad (4)$$

The breakup of the bonds in the CH_3COO^- ligands at a higher temperature will release CH_4, CO, and H_2 according to the following equation, finally resulting the huge weight loss:

$$CH_3COO^- \xrightarrow{heat} CH_4 + CO + H_2 \quad (5)$$

The peak between approximately 1041°C and 1348°C, and over 1348°C can be attributed to the crystallization of LTA powders. From the TGA-DSC results, the calcination temperature of LTA can be set from 1100°C to 1400°C. Therefore, the calculation steps are: drying sol at temperature below 125°C, calcining xerogel at 300°C for 2h to remove organics, holding at 650°C to avoid self-igniting the citric acid, then calcination at the target temperature for 2h to crystallize LTA.

3.2. The morphology of as-calcined LTA powders

The morphology of as-calcined LTA powders is shown in Figure 3. There are two kinds of morphologies of LTA powders. Figure 3 (a) and (b) show the porous structure of LTA powders which consist of nanoparticles, nano needle-like structure (can also be called nanowhiskers), and micropores. This structure

is difficult to separate into small particles even after 24h of ball milling. The nano particles form the frame of the micro pores, with most of the nanowhiskers are located at the bottom of pores. This may be because the second calcination step at 650^{o}C is the nucleation temperature of γ-Al_2O_3, which normally shows a needle-like structure. The main component of LTA is Al_2O_3, so it is possible that parts of the γ-Al_2O_3 nucleated and grew during the holding time. At a higher calcination temperature (900^{o}C), the morphology of γ-Al_2O_3 is in particulate form so the powders consist of nanowhiskers and nanoparticles [18]. The porous structure may be due to the high drying temperature in the first calcination step which exceeded the boiling point of the solvent, leading to fast evaporation and resulting in this porous structure of the LTA powders.

LTA powders with a porous structure are not desirable for property study because the porous structure is difficult to remove. Thus, during the bulk and coating preparation process, there will be more pores inside the bulk or coating samples that exceed the proper porosity, which are undesirable for further study, especially for their mechanical properties. Furthermore, holding the xerogel at 650^{o}C may lead to composition segregation due to the preferred growth of γ-Al_2O_3.Therefore, it is necessary to avoid obtaining LTA powders with a porous structure.

Dense LTA powders were obtained by modifying the three-step calcination to a two-step calcination process [see Figure 3 (c) and (d)]. The two-step calcination was calcined at 300^{o}C for 2h and subsequently heated up to 1350^{o}C for a further 2h to avoid nucleation of γ-Al_2O_3. The drying temperature was also changed to 65^{o}C, which is lower than the boiling point of ethanol. As a result, dense platelets consisting of only small LTA grains around 300nm without any

porous structure and whiskers were produced [see Figure 3 (c) and (d)]. Hence, the fine LTA powders were synthesized via the sol-gel route.

3.3. The characteristics of sol-gel produced LTA powders

XRD patterns of LTA powders calcined at different temperatures are shown in Figure 4. Figure 4 (b) shows that the LTA powders are amorphous and crystalline when calcined at 950^{o}C for 2h. Although LTA can be obtained when the calcination temperature is increased to 1100^{o}C and above according to the XRD patterns shown in Figure 4 (c) to (e), the XRD patterns of LTA calcined at 1100^{o}C and 1200^{o}C are not well-matched with the JCPDS card 37-1233 for LTA [Figure 4 (a)] to some degree. Only the XRD patterns of LTA calcined at 1350^{o}C fully match the JCPDS card, which indicates that single phase LTA can be obtained at this temperature. Therefore, the calcination temperature for the crystallization of LTA was set to 1350^{o}C.

The crystallite sizes of LTA calcined at different temperatures were calculated using the Scherrer formula:

$$D = \frac{\kappa\lambda}{\beta\cos\theta} \tag{6}$$

where κ is a constant which is 0.89; D represents crystallite size (nm); β represents Full Width Half Maximum (FWHM) which should be converted to radian(rad) during calculation; θ is the diffraction angle (^{o}) and λ is the wavelength of X-ray, which is normally 0.154056nm.

The calculated results show that amorphous LTA has an extremely small average crystallite size of approximately 5.6nm, with the crystallite size increasing as the calcination temperature increases, circa. 32nm for calcination at 1100^{o}C, 38nm for 1200^{o}C, and 50nm for 1350^{o}C. The grain size obtained from TEM graphs (in Figure 5) accord with the calculated results, with the grain

size of LTA calcined at 1350^{o}C being circa 250nm, whilst at a lower calcination temperature of 1100^{o}C and 1200^{o}C, the grain size of LTA is approximately 150nm.

Information on the crystal structure of LTA was obtained from the Crystal Structure Depot at FIZ Karlsruhe-Leibniz Institute for Informationsinfrastruktur, which was plotted by Diamond (see Figure 6). As reported, LTA is a face-centred monoclinic structure with a huge unit cell interleaved with pseudobrookite-like layers [9, 19]. Such a large unit cell formed by 248 atoms has a very complex 3D framework, which has been reported to fundamentally consist of AlO_6 and TiO_6 octahedra, connected through AlO_4 tetrahedra and 12-fold-coordinated La^{3+} cations[19].

3.4. The thermochemical stability of sol-gel produced LTA

A potential thermal barrier material must have good chemical stability with the thermally grown oxide (TGO) under high temperature exposure, particularly for Al_2O_3 (the main composition of TGO) to achieve long-term application time. Figure 7 shows the XRD patterns of sol-gel produced LTA mixed with α-Al_2O_3 calcined at 1500^{o}C for 10h. All the patterns in Figure 7 matching α-Al_2O_3 (marked rhombus) and LTA (other peaks) indicate no apparent reaction between LTA and α-Al_2O_3 at 1500^{o}C. Therefore, it can be concluded that sol-gel synthesized LTA has good thermochemical stability at temperatures up to 1500^{o}C.

3.5. The coefficients of thermal expansion of LTA

CTE is one of the important properties for TBC materials and is a key factor in determining the suitability of new materials as TBC materials. The typical CTEs of the Ni-based substrate and the metallic bond coat are circa. 16.3×10^{-6} $^{o}C^{-1}$ and 15.5×10^{-6} $^{o}C^{-1}$, respectively, while the CTEs of the state-of-the-art industrial

TBC material 8YSZ are approximately $11\times10^{-6}\ ^{o}C^{-1}$. The big gap in the CTEs between the metallic parts and ceramic coats will introduce stresses during thermal cycling and accelerate the failure of the TBC system.

The CTE curves of as-calcined LTA ceramics produced by both solid state reaction and the sol-gel method are shown in Figure 8. It can be clearly seen that the CTEs of sol-gel synthesized LTA ceramic are higher than those of the solid state reaction synthesized LTA ceramic at temperatures above 200^{o}C, approximately $10.2\times10^{-6}\ ^{o}C^{-1}$ and $9.3\times10^{-6}\ ^{o}C^{-1}$ at 950^{o}C, respectively. This is because the CTE is a size-dependent property of a material [20, 21], with it being reported that the conventional thermal barrier materials 8YSZ in nanostructure form might improve the performance of TBCs by having lower thermal conductivity, higher CTE, and excellent mechanical properties [12, 22, 23]. Theoretically, it can be explained by the idea ‘nanostructure=bulk + surface’ [24, 25]. When compared with the equilibrium bulk atoms, atoms on the surface or interface (such as a grain boundary) of a crystal are not saturated with respect to their bonding state, with their coordination number also less than that for bulk atoms. The relationship between potential energy and interatomic spacing is shown in Figure 9, indicating that surface/interface atoms show less deep potential energy minimum well than for bulk atoms. Due to this, vibrational kinetic energy for the surface/interface and bulk atoms also shows consequences of a different extent. Evidently, the less deep potential energy minimum for surface/interface atoms makes the position variation larger, due to the thermal vibration, when compared to that for bulk atoms. Therefore, in consideration of the asymmetry of the potential energy minimum wells, the surface/interface atoms of a crystal show larger thermal expansion than that for bulk atoms. Other reported work [26] proved that the surface/interface atoms

show less deep potential energy wells and even more asymmetry than bulk atoms. The smaller the crystal size, the larger the ratio of the number of surface/interface atoms and the number of bulk atoms. Thus, the variation in the CTE of a nanostructure varies inversely in accordance with the size of the nanostructure, in other words, the smaller the crystallite size, the larger the average CTE.

As the temperature is increased, the amplitude of phonon vibration increases. The higher the temperature, the more phonons are in the crystal lattice, and the greater the amplitude of the crystal lattice vibration. At high temperatures, not only can low-frequency phonons get excited, but the high-frequency phonons are also get excited, leading to more intense vibration in the crystal lattice than when subjected to low temperatures. Intense vibration makes the average distance of mass points much larger and increases the effect of crystallite size on CTEs. This is why the differences in CTEs become larger at a high temperature and the CTEs show a rising tendency when accompanied by an increase in temperature.

4. Conclusions

It can be concluded that the single phase nanostructured LTA has been synthesized successfully at 1350^{o}C, which is lower than solid state synthesized LTA (1500^{o}C). Fine LTA powders can be obtained by two-step calcination with suitable drying temperature for the sol, with such fine powders suitable for the APS deposition after spray drying or ingots for the EB-PVD process. The crystallite sizes of nanostructured LTA are circa. 50nm (calculated using the Scherrer formula), which is much smaller than those synthesized by solid state reaction, and the growth tendency of grain size accords with the growth tendency of crystallite size. The thermochemical stability of LTA is excellent and

they do not react with Al_2O_3 up to 1500^oC. CTEs of nanostructured LTA are higher than micron size LTA because CTE is a size-dependent property. Sol-gel synthesized LTA is a promising precursor material for the fabrication of high-temperature thermal barrier materials and luminescent materials.

Acknowledgement

Peng Zhang would like to thank the China Scholarship Council for the support of living expense and scholarship from the University College London and the University of Nottingham.

References

[1] N.P. Padture, M. Gell, E.H. Jordan, Thermal barrier coatings for gas-turbine engine applications, Science, 296 (2002) 280-284.

[2] M.N. Rahaman, J.R. Gross, R.E. Dutton, H. Wang, Phase stability, sintering, and thermal conductivity of plasma-sprayed ZrO_2–Gd_2O_3 compositions for potential thermal barrier coating applications, Acta Materialia, 54 (2006) 1615-1621.

[3] J. Xiang, S. Chen, J. Huang, H. Zhang, X. Zhao, Phase structure and thermophysical properties of co-doped $La_2Zr_2O_7$ ceramics for thermal barrier coatings, Ceramics International, 38 (2012) 3607-3612.

[4] T.D. Bennett, F. Yu, A nondestructive technique for determining thermal properties of thermal barrier coatings, Journal of applied physics, 97 (2005) 013520-013520-013512.

[5] W. Ma, S. Gong, H. Li, H. Xu, Novel thermal barrier coatings based on $La_2Ce_2O_7$/8YSZ double-ceramic-layer systems deposited by electron beam physical vapor deposition, Surface and Coatings Technology, 202 (2008) 2704-2708.

[6] D. Basu, C. Funke, R. Steinbrech, Effect of heat treatment on elastic properties of separated thermal barrier coatings, Journal of materials research, 14 (1999) 4643-4650.

[7] X. Cao, R. Vassen, D. Stoever, Ceramic materials for thermal barrier coatings, Journal of the European Ceramic Society, 24 (2004) 1-10.

[8] R. Vassen, X. Cao, F. Tietz, D. Basu, D. Stöver, Zirconates as new materials for thermal barrier coatings, Journal of the American Ceramic Society, 83 (2000) 2023-2028.

[9] X. Xie, H. Guo, S. Gong, H. Xu, Lanthanum–titanium–aluminum oxide: a novel thermal barrier coating material for applications at 1300^{o}C, Journal of the European Ceramic Society, 31 (2011) 1677-1683.

[10] R. Lima, B. Marple, Nanostructured YSZ thermal barrier coatings engineered to counteract sintering effects, Materials Science and Engineering: A, 485 (2008) 182-193.

[11] B. Kear, Z. Kalman, R. Sadangi, G. Skandan, J. Colaizzi, W. Mayo, Plasma-sprayed nanostructured Al_2O_3/TiO_2 powders and coatings, Journal of thermal spray technology, 9 (2000) 483-487.

[12] M. Gell, Application opportunities for nanostructured materials and coatings, Materials Science and Engineering: A, 204 (1995) 246-251.

[13] J. Karthikeyan, C. Berndt, J. Tikkanen, S. Reddy, H. Herman, Plasma spray synthesis of nanomaterial powders and deposits, Materials Science and Engineering: A, 238 (1997) 275-286.

[14] X. Cao, Thermal Barrier Coating Materials, Science Press, Beijing, 2007.

[15] Y.-L. Chai, Y.-S. Chang, G.-J. Chen, Y.-J. Hsiao, The effects of heat-treatment on the structure evolution and crystallinity of $ZnTiO_3$ nano-crystals prepared by Pechini process, Materials Research Bulletin, 43 (2008) 1066-1073.

[16] C. Pouchert, J. Behnke, Non‐aromatic esters and lactones, The Aldrich Library of 13C and 1H FTNMR Spectra, 1st Ed.; Aldrich Publications: Milwaukee, WI, 1 (1993) 973.

[17] D. Hennings, W. Mayr, Thermal decomposition of (BaTi) citrates into barium titanate, Journal of Solid State Chemistry, 26 (1978) 329-338.

[18] S. Tao, Prepartion and characterization of alumina nanocrystalline powder by complexing sol-gel method, Journal of the Chinese ceramic society, Vol.37, No.4 (2009).

[19] M. Kasunič, A. Meden, S.D. Škapin, D. Suvorov, A. Golobič, Structure of $LaTi_2Al_9O_{19}$ and reanalysis of the crystal structure of $La_3Ti_5Al_{15}O_{37}$, Acta Crystallographica Section B: Structural Science, 67 (2011) 455-460.
[20] Y. Kuru, M. Wohlschlögel, U. Welzel, E. Mittemeijer, Crystallite size dependence of the coefficient of thermal expansion of metals, Applied physics letters, 90 (2007) 243113.
[21] S. Pathak, V.B. Shenoy, Size dependence of thermal expansion of nanostructures, Physical Review B, 72 (2005) 113404.
[22] B. Kear, G. Skandan, Thermal spray processing of nanoscale materials: Davos, Switzerland, August 4–8, 1997, Nanostructured Materials, 8 (1997) 765-769.
[23] H. Chen, X. Zhou, C. Ding, Investigation of the thermomechanical properties of a plasma-sprayed nanostructured zirconia coating, Journal of the European Ceramic Society, 23 (2003) 1449-1455.
[24] J.R. Nicholls, K. Lawson, A. Johnstone, D. Rickerby, Methods to reduce the thermal conductivity of EB-PVD TBCs, Surface and Coatings Technology, 151 (2002) 383-391.
[25] R.E. Miller, V.B. Shenoy, Size-dependent elastic properties of nanosized structural elements, Nanotechnology, 11 (2000) 139.
[26] M. Kiguchi, T. Yokoyama, D. Matsumura, H. Kondoh, O. Endo, T. Ohta, Surface structures and thermal vibrations of Ni and Cu thin films studied by extended x-ray-absorption fine structure, Physical Review B, 61 (2000) 14020.
[27] U.o. Cambridge, Origin of thermal expansion, University of Cambridge.

List of figure captions

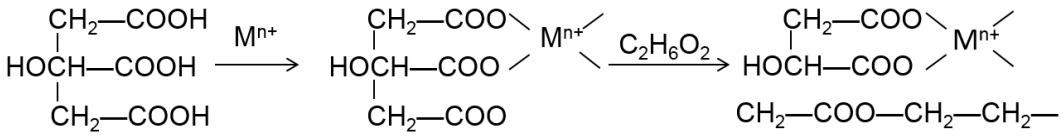

Figure 1 The reaction process of synthesizing nanopowders by Pechini sol-gel method

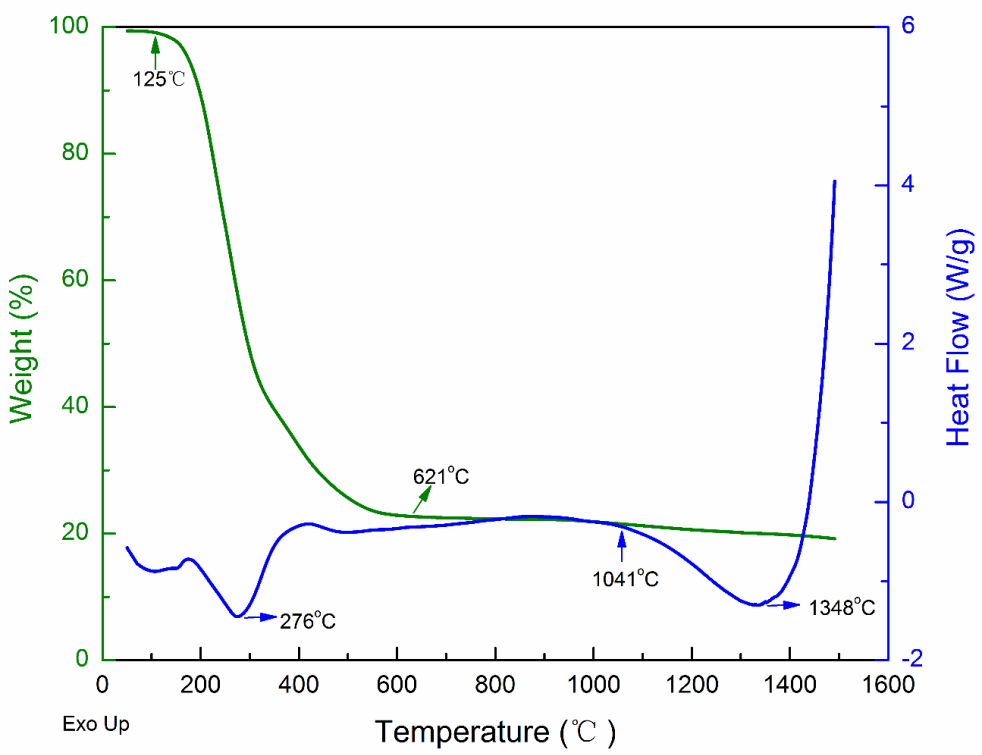

Figure 2 TGA-DSC curves of LTA xerogel

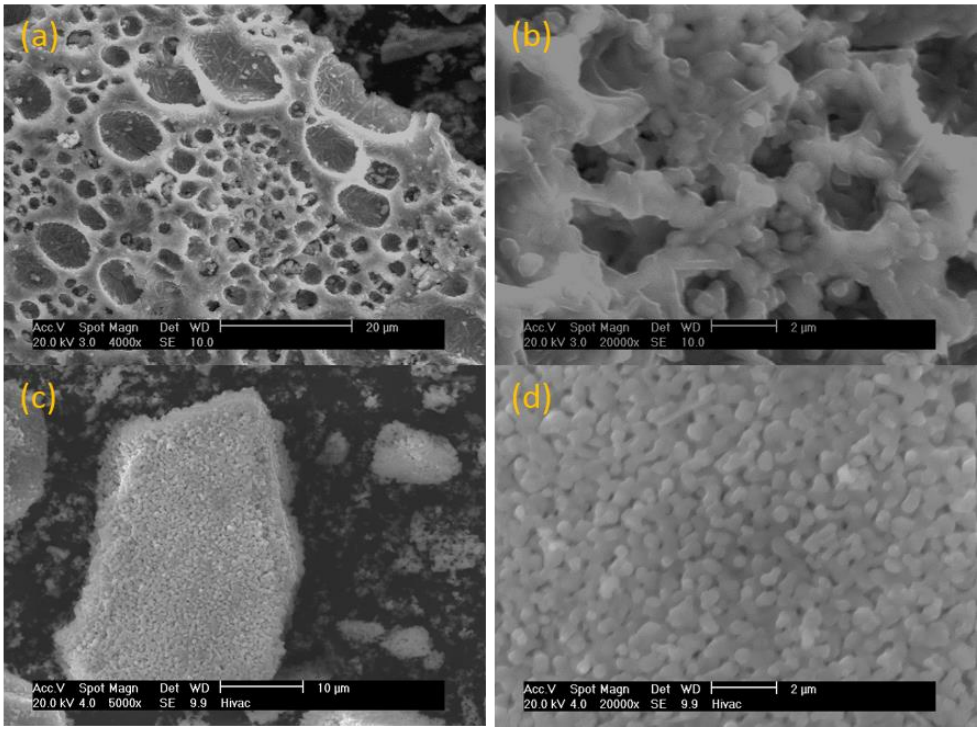

Figure 3 Two types of sol-gel produced LTA powders without ball milling (a) porous platelet LTA powders and details of powders (b), (c) dense LTA powders and details of powders (d)

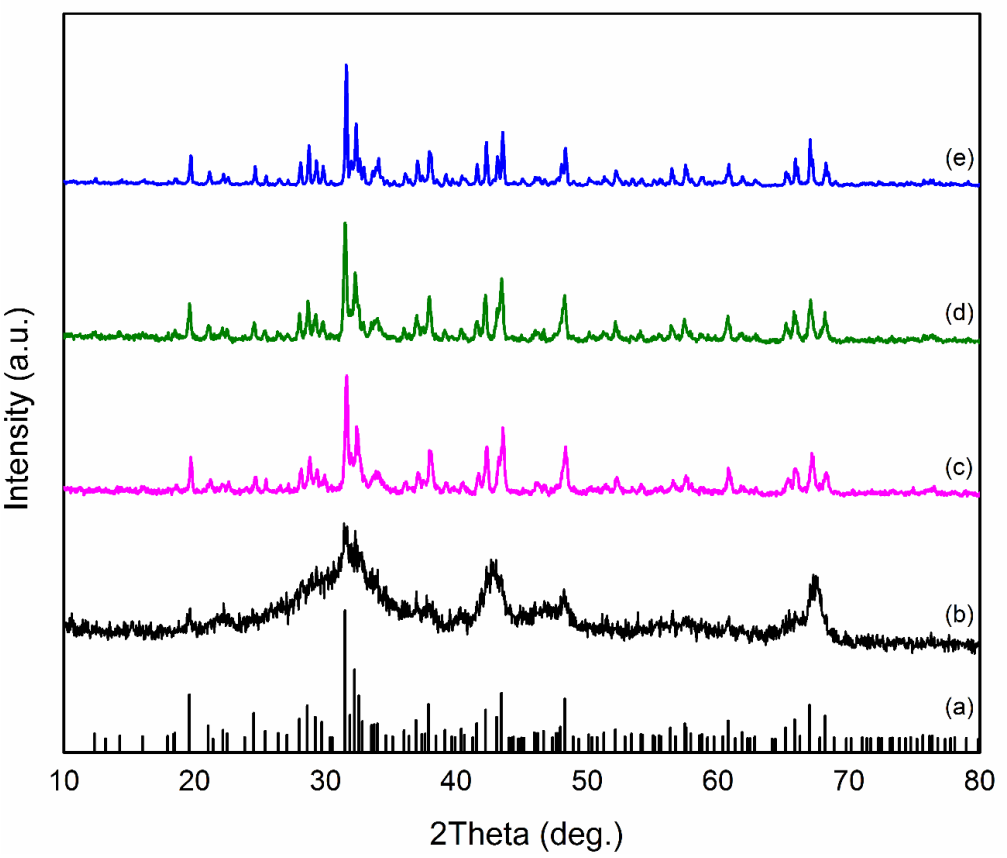

Figure 4 XRD patterns of sol-gel produced LTA calcined at different temperature: (a) JCPDS card 37-1233, (b) 950°C, (c) 1100°C, (d) 1200°C, (e) 1350°C

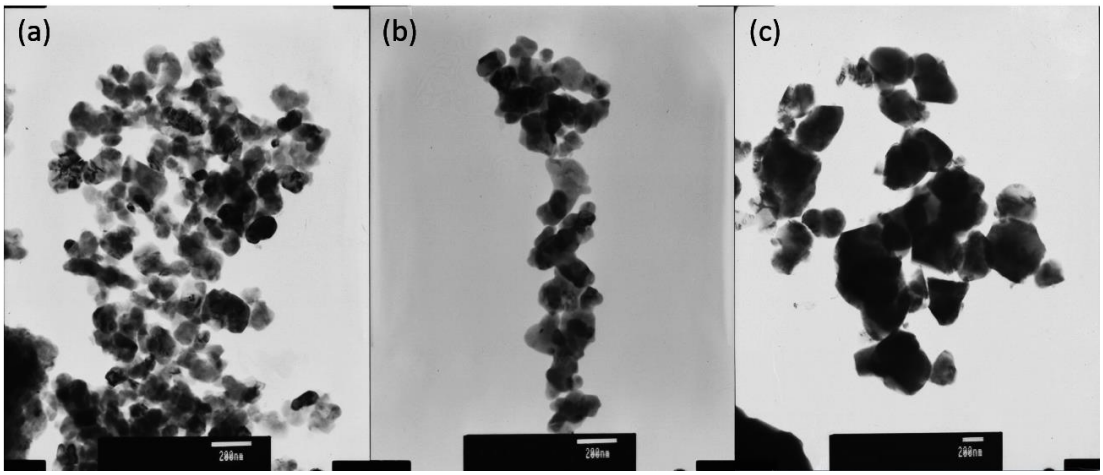

Figure 5 TEM morphology of LTA calcining at different temperature: (a) 1100°C, (b) 1200°C, (c) 1350°C

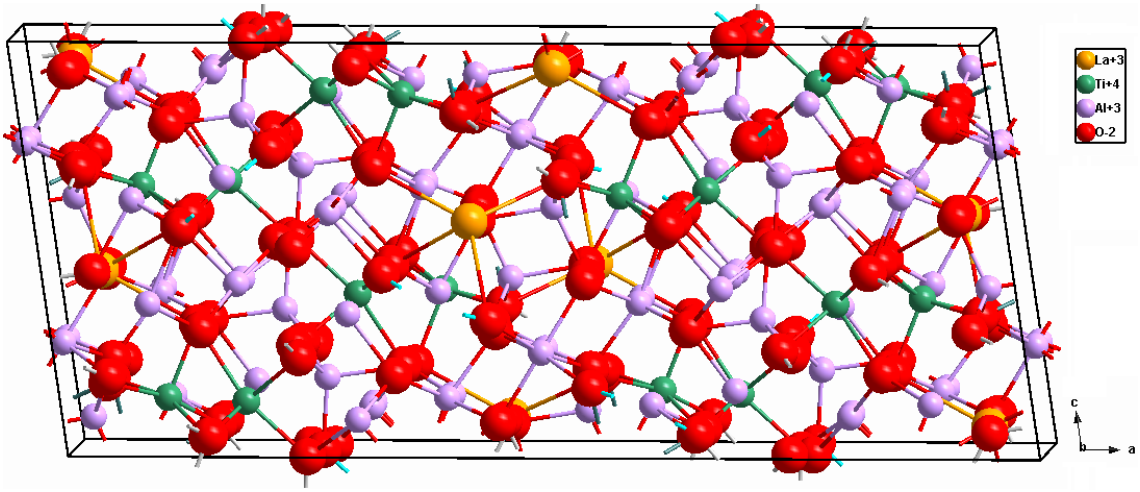

Figure 6 The crystal structure of LTA

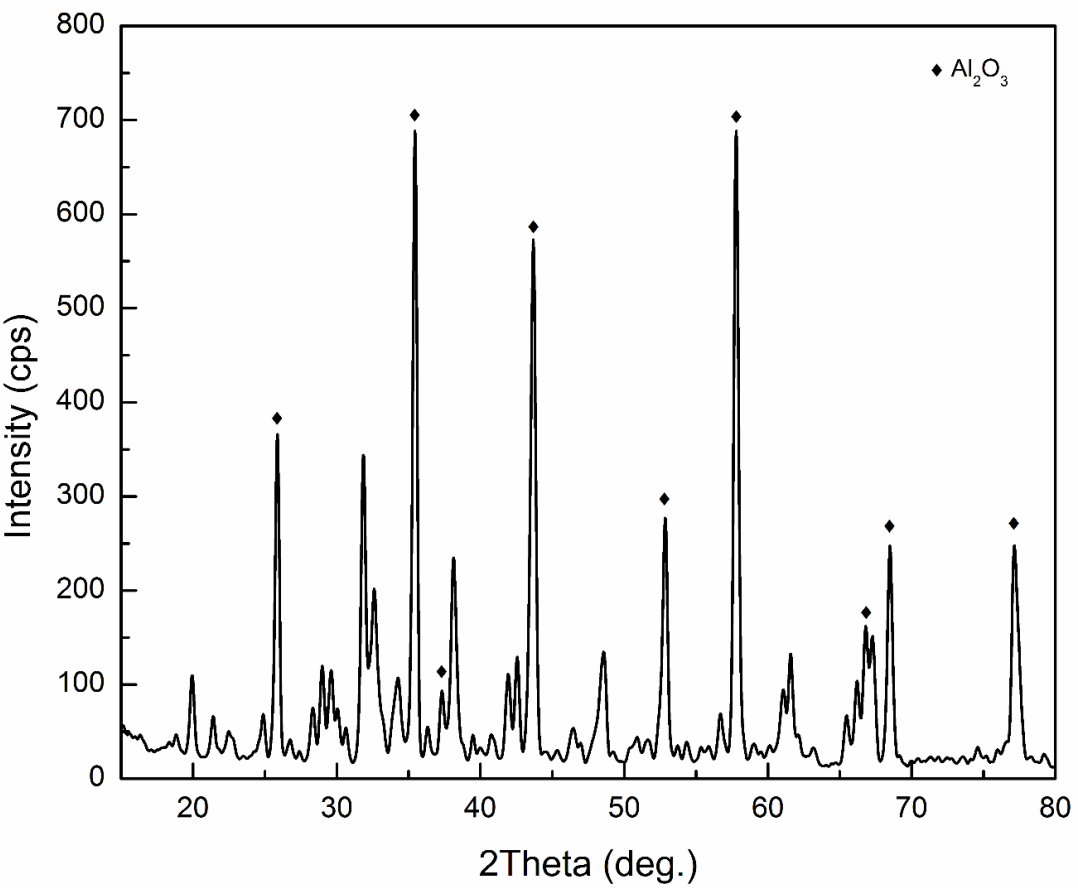

Figure 7 XRD patterns of cold-pressed sol-gel produced LTA bulk under 10 h heat-treatment at 1500°C: Al_2O_3 phase is marked rhombus and rest of phase are LTA phase

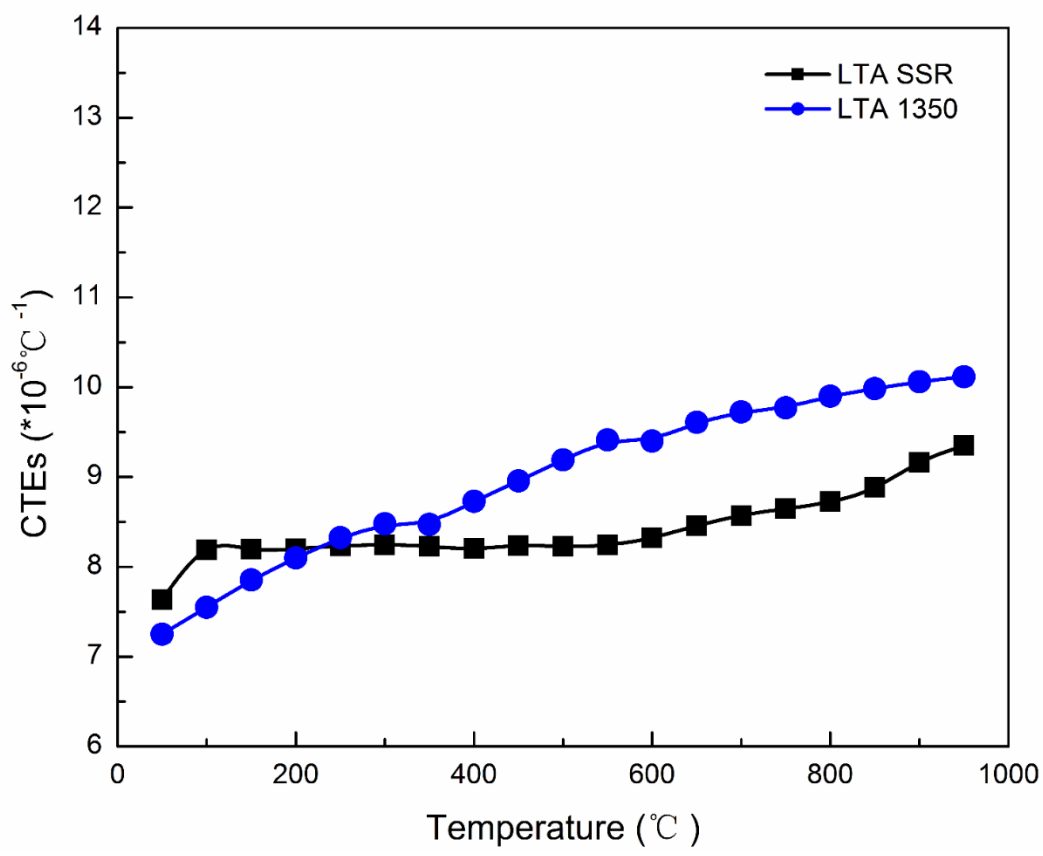

Figure 8 CTEs of LTA prepared by solid state reaction calcined at 1500°C and sol-gel calcined at 1350°C

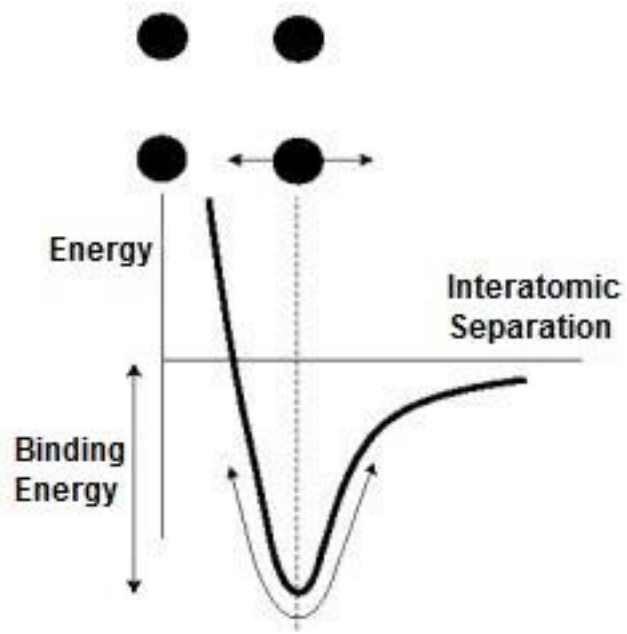

Figure 9 Schematic of the dependence of potential energy of an atom within a solid on the interatomic spacing[27]